Macromolecules

ARTICLE

pubs.acs.org/Macromolecules

Orthogonal Crystal Orientation in Double-Crystalline Block Copolymer

Ming-Champ Lin,[†] Yi-Chin Wang,[†] Jean-Hong Chen,[‡] Hsin-Lung Chen,*[,†] Alejandro J. Müller,*[,§] Chun-Jen Su,[∥] and U-Ser Jeng[∥]

[†]Department of Chemical Engineering and Frontier Research Center on Fundamental and Applied Sciences of Matters, National Tsing Hua University, Hsin-Chu 30013, Taiwan

[‡]Department of Polymer Materials, Kun Shan University, Tainan Hsien 71103, Taiwan

[§]Departamento de Ciencia de los Materiales, Grupo de Polímeros USB, Apartado 89000-A, Caracas, Venezuela

[∥]National Synchrotron Radiation Research Center, Hsin-Chu 300, Taiwan

Supporting Information

ABSTRACT: In this study, we explore the orientation of crystals formed within the lamellar domains of a diblock copolymer composed of two crystallizable blocks, that is, poly(L-lactide)-*block*-polyethylene (PLLA-*b*-PE). The orientation of both PLLA and PE crystals with respect to the lamellar interface was examined under two types of crystallization condition with a broad range of crystallization temperatures (T_c). The first type was the "two-stage crystallization", where the PLLA block was allowed to crystallize before PE. The second was the "one-stage crystallization", where PLLA and PE blocks competed to crystallize. A homeotropic crystal orientation was always observed for the PLLA crystals, with the crystalline stems lying parallel to the lamellar normal regardless of the crystallization condition, except when T_c approached the glass-transition temperature of PLLA, where the orientation became random. A homogeneous crystal orientation with the PE crystalline stems oriented perpendicular to the lamellar normal was always identified at low-to-intermediate degree of undercooling, whereas at large undercooling, the crystals showed random orientation. The "orthogonal orientation" disclosed here was preserved over a broad range of undercooling. Our results further demonstrated that the orientation of both PLLA and PE crystals depended mainly on T_c but was independent of the competitiveness of the two crystallization processes. This was a consequence of the strong segregation that made the two blocks crystallize independently within their respective microdomains.

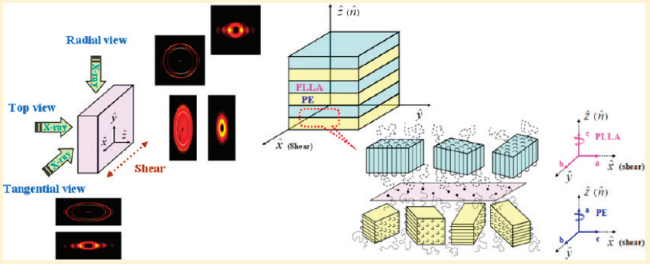

INTRODUCTION

Block copolymers are attractive building blocks for constructing nanostructures by self-assembly.[1−3] Their structural formation occurs through a microphase separation between incompatible constituting chains, and the morphology of the microdomains thus formed is governed by the strength of interblock repulsion and volume fraction.[4] The spatial arrangement of the microdomains is characterized by certain macrolattices, including 1-D array for lamellar microdomains, 2-D hexagonal lattice for cylindrical domains, and 3-D BCC lattice for spherical domains. At the molecular level, the block chains within the microdomains are typically liquid-like without distinct molecular order.

Incorporation of crystallization into the self-organization mechanism of block copolymers to generate a hierarchically ordered structure may enrich their morphology and properties.[5−8] The presence of molecular order, which may be mesomorphic or crystalline in nature, leads to a structural hierarchy in the system; namely, the copolymer displays a long-range ordered arrangement of microdomains on a larger length scale and another characteristic ordering of chains at the molecular level. "Structure-within-structure" or "order-within-order" are the appropriate terms to describe such a morphological feature. Crystalline molecular order, in particular, can be accessed conveniently by introducing one or more crystallizable polymers into the block copolymer architecture to yield interesting directional control of mechanical, thermal, and optical properties from the anisotropic nature of polymer chains forming the crystals.

For directional control of properties, the manipulation of the orientation of crystals (represented by the direction of crystalline stems) with respect to the interface of microdomains is the most important fundamental task. It has been recognized for block copolymers composed of one crystalline and one amorphous block (i.e., the "crystalline−amorphous" block copolymers) that the crystals formed within microdomains can exhibit certain preferred orientation with respect to the interface.[9] In the case of lamellar[9−16] and cylindrical domains,[17−20] the alignment of crystalline stems may be perpendicular or parallel to the interface.

Received: May 16, 2011
Revised: July 5, 2011
Published: August 15, 2011

The former is called "homeotropic orientation", whereas the latter is termed "homogeneous orientation", as adopted from the terminology used for describing the alignment of liquid crystalline molecules on substrate. Although the crystal orientations in many crystalline−amorphous block copolymers have been revealed, the key factors dictating the alignment of crystalline stems are not well understood. It appears that the spatial confinement imposed by the domain interface, the tethering density associated with the junction point constraint, the chain stretching near the interface, and the mechanism of nucleation are all important parameters.[16,21−23]

In this study, we investigate the coexistence of two distinct types of crystal orientations established by the two crystalline blocks in a "crystalline−crystalline block copolymer". The crystalline structure formation in this type of system is expected to be more complex than the crystalline−amorphous counterpart because of the potential interplay between the two crystallization processes occurring within the respective microdomains.[24,25] In general, if the crystallization rates of the two blocks are sufficiently different, then the component with faster crystallization would crystallize first, and the crystallization of the other block then proceeds under the spatial environment prescribed by the leading component (i.e., the crystallization is sequential).[26−33] If the crystallization rates of the two blocks are similar, then competitive or interactive crystallization may take place.[34−40]

The system studied here is a poly(L-lactide)-*block*-polyethylene (PLLA-*b*-PE). The symmetric composition coupled to large segregation strength prescribes the crystallizations of the two blocks to occur within the nanoscale lamellar microdomains without forming spherulites. Moreover, the relatively large disparity in melting points ($T_m^{PLLA} \approx 172$ °C, $T_m^{PE} \approx 104$ °C) and glass-transition temperatures ($T_g^{PLLA} \approx 62$ °C, $T_g^{PE} \approx -100$ °C) between these two components allows the system to crystallize over a broad range of crystallization conditions for tuning the competitiveness of the two crystallization events. In this work, we use 2D small-angle X-ray scattering (SAXS) and wide-angle X-ray diffraction (WAXD) techniques to resolve the orientations of PLLA and PE crystals with respect to the lamellar interface under different crystallization conditions. It will be shown that the two types of crystals normally exhibited the "orthogonal orientation", where the PE crystals displayed homogeneous orientation, whereas PLLA crystals showed homeotropic orientation. Exceptions were observed when the degree of undercooling was large, where the orientations of both crystals were random.

EXPERIMENTAL SECTION

Material. The synthesis of PLLA-*b*-PE used in this study has been described in previous publications.[41] In brief, 1,3-butadiene was anionically polymerized in cyclohexane using *sec*-butyllithium as the initiator and subsequently end-capped with ethylene oxide to give hydroxyl-terminated 1,4-polybutadiene containing ca. 93% of the 1,4-regioisomer. This polybutadiene was then hydrogenated to give hydroxyl-terminated polyethylene, which was utilized in combination with $AlEt_3$ as a macroinitiator in the ring-opening polymerization of L-lactide (PLLA). Because the PE block has been prepared from hydrogenating a 1,4-polybutadiene, it can be considered to be a random copolymer of ethylene and butene (with a low butene content of ∼7 wt %). The molecular weights of PLLA and PE blocks were 23k and 27k (g/mol), respectively, determined by proton nuclear magnetic resonance (^{1}H NMR); hence, the volume fraction of the constituting PLLA block was 0.4, prescribed by the corresponding molecular weights and the relevant densities of PLLA and PE blocks in the melt state. The polydispersity of this copolymer was found to be 1.06, and such a low index resulted in the formation of highly ordered lamellar microdomains. Detailed molecular characteristics and the thermal properties of this diblock copolymer have been addressed elsewhere.[41−44]

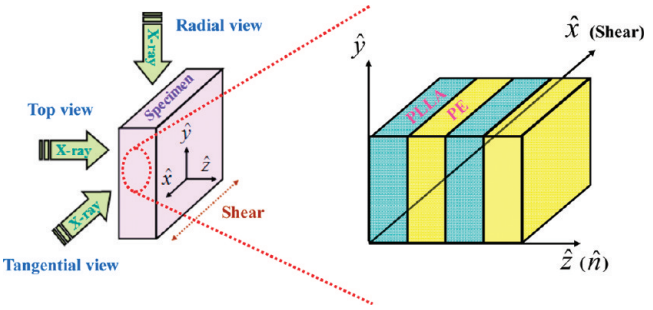

Figure 1. Schematic illustrations of the geometry of shear-oriented PLLA-*b*-PE specimen, indicating different incident directions of the X-ray for obtaining the 2-D scattering patterns in tangential-view (the X-ray beam is traveling along $\hat{x}$), radial-view (the X-ray is along $\hat{y}$), and top-view (the X-ray is along $\hat{z}$). The illustration on the right shows the alignment of the lamellar microdomains attained after the shear treatment.

Sample Preparation. The copolymer samples for the crystallization studies were prepared by solvent casting. The copolymer was dissolved in toluene at 65 °C, yielding a 5% (w/v) solution. The solvent was evaporated slowly at 70 °C, followed by further drying under vacuum at 70 °C for 2 days to remove the residual solvent.

Large-Amplitude Oscillatory Shear Experiment. Large-amplitude oscillatory shear (LAOS) was performed to produce large-scale alignment of the microdomains in PLLA-*b*-PE. The shear was carried out with a Linkam CSS 450 shear hot stage in the oscillatory mode with the shear frequency of 0.3 Hz and the strain amplitude of 70%. The samples with the size of 5.0 × 5.0 × 0.2 mm^3 were subjected to LAOS for 2 h under a nitrogen atmosphere at 150 °C. This temperature was found to be the optimum one to produce good alignment of the lamellar microdomains, although it was lower than T_m^{PLLA}. (Shearing at temperatures above T_m^{PLLA} caused thermal degradation of the samples.) To erase the thermal history associated with the occurrence of PLLA crystallization during LAOS treatment, we annealed all sheared samples at 190 °C for 15 min before cooling to the prescribed temperature for crystallization.

After the LAOS treatment, the shear direction was marked on the surface of the sample. The specimen was then cut into rectangular shape with one side directing along the shear direction and the other side perpendicular to the shear direction, as schematically illustrated in Figure 1. The shear direction is denoted as $\hat{x}$, the vorticity direction (which is perpendicular to the shear direction in the shear plane) is indicated as $\hat{y}$, and the gradient direction is along $\hat{z}$. It will be shown that the lamellar normal ($\hat{n}$) directed along the $\hat{z}$ axis.

Crystallization Treatment. The samples after shearing were further treated under prescribed crystallization conditions. For the two-stage crystallization process, the shear-oriented sample was annealed at 190 °C in a Linkam HFS 91 hot stage for 15 min to erase the residual stresses and thermal histories. Meanwhile, another Linkam hot stage was preset at a specific crystallization temperature (i.e., T_c = 120 °C, which was higher than T_m^{PE} but lower than T_m^{PLLA}). After 15 min, the annealed sample was promptly transferred to the second hot stage to allow PLLA crystallization. When PLLA crystallized to saturation, the sample was subsequently transferred from the Linkam hot stage

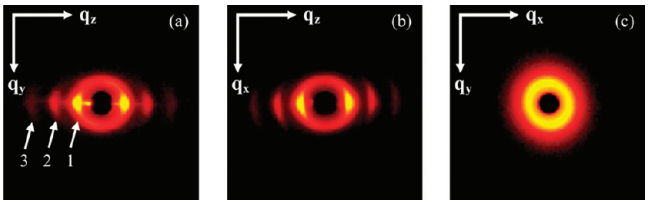

Figure 2. Two-dimensional SAXS patterns of shear-oriented PLLA-*b*-PE subjected to a two-stage crystallization process. The system was cooled from 190 to 120 °C to allow PLLA crystallization, followed by cooling to T_c^{PE} = 97 °C to induce PE crystallization. (Similar scattering patterns were observed for T_c^{PE} = 45−80 °C.) (a) Tangential view, (b) radial view, and (c) top view.

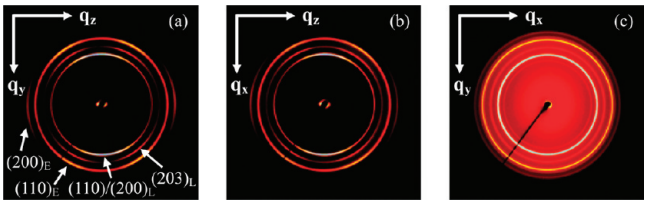

Figure 3. Two-dimensional WAXD patterns of shear-oriented PLLA-*b*-PE subjected to a two-stage crystallization process. The system was cooled from 190 to 120 °C to allow PLLA crystallization, followed by cooling to T_c^{PE} = 97 °C to induce PE crystallization. (Similar scattering patterns were observed for T_c^{PE} = 45−80 °C.) (a) Tangential view, (b) radial view, and (c) top view. The subscripts L and E marked in the (*hkl*) diffraction planes signify PLLA and PE, respectively.

to the DSC sample chamber, which was pre-equilibrated at the prescribed T_c. Similarly, for the one-stage crystallization process, the sample after annealing at 190 °C was directly transferred from the hot stage to the DSC preset at the specific T_c for isothermal crystallization. All samples were kept at the specific temperature for a sufficiently long time to crystallize to saturation before SAXS/WAXD measurement.

X-ray Scattering Experiments. For the X-ray scattering experiment, three patterns were collected for each sample by rotating the specimen to allow for the incident X-ray to pass through the three principal axes of the specimen. That is, the tangential-, radial-, and top-view patterns of each film were collected by having the incident X-ray traveling along the shear direction ($\hat{x}$), vorticity direction ($\hat{y}$), and film normal ($\hat{z}$), respectively. (See Figure 1.)

SAXS experiments were performed at station BL23A1 at the National Synchrotron Radiation Research Center (NSRRC) located at Hsin-Chu, Taiwan.[45] The energy of X-ray source and sample-to-detector distance were 8 keV (λ = 0.155 nm) and 2259 mm, respectively. A 2-D Mar CCD detector with 512 × 512 pixel resolution was used to record the scattering pattern.

The WAXD measurements were performed at station BL17A1 at the NSRRC using an imaging plate as the detector. The X-ray beam with the wavelength of 1.334 Å was collimated into the beam size of 0.5 mm × 3 mm by two slits separated by 1.1 mm. With a sample-to-detector distance of 212 mm, the diffraction patterns in tangential, radial, and top view were collected over the q range of 1 to 34 nm^{-1}.

■ RESULTS AND DISCUSSION

To reveal the crystal orientations in double-crystalline PLLA-*b*-PE diblock copolymer, we first shear-oriented the sample at 150 °C for 2 h to produce a large-scale alignment of the microdomains in the sample, followed by annealing at 190 °C to eliminate residual stresses and thermal history. The sample was then treated by different thermal conditions to allow for PLLA and PE crystallization.

Here we have examined the orientation of crystals formed under two types of conditions. The first type is called "two-stage crystallization", where the system was cooled from 190 °C (which is higher than both T_m^{PE} and T_m^{PLLA}) to T_c^{PLLA} = 120 °C ($T_m^{PE} < T_c^{PLLA} < T_m^{PLLA}$) to allow PLLA crystallization, followed by cooling to prescribed temperatures (i.e., T_c^{PE} = −50 to 97 °C and also direct immersion into liquid nitrogen) to induce PE crystallization. The other type is called "one-stage crystallization", where the system was cooled directly from 190 °C to the prescribed temperatures ($T_c < T_m^{PE}$), at which the competitive crystallization of PLLA and PE blocks was anticipated.

Crystal Orientation Displayed under Two-Stage Crystallization. Figure 2 shows the 2D SAXS patterns of shear-oriented PLLA-*b*-PE subjected to a two-stage crystallization process with T_c^{PE} = 97 °C for the second stage. (Similar results were observed for T_c^{PE} = 45−80 °C.) Both tangential- (Figure 2a) and radial-view (Figure 2b) patterns displayed mainly three reflections with the position ratio of 1:2:3 on the equator, indicating that a lamellar morphology with an interlamellar distance of 78 nm was formed. This value was quite similar to that in the melt and thus ensured that the crystallizations of both PLLA and PE blocks were effectively confined within their respective lamellar microdomains.[44] The scattering features also revealed that the lamellar microdomains formed in PLLA-*b*-PE were macroscopically aligned parallel to the $\hat{x} - \hat{y}$ plane, as schematically presented in Figure 1.

Figure 3 shows the corresponding 2D WAXD patterns of PLLA-*b*-PE subjected to a two-stage crystallization at T_c^{PE} = 97 °C. (Similar WAXD patterns were also observed for T_c^{PE} = 45−80 °C.) In the tangential- and radial-view patterns, the diffraction arcs observed at first meridian (q = 11.7 nm^{-1}) and the second quadrant (q = 13.4 nm^{-1}) were associated with the (110)/(200) and (203) diffractions of PLLA crystals, respectively. In the azimuthal scans (obtained by scanning the intensity of a specific diffraction around the azimuthal angle starting from the vertical direction of the pattern) of PLLA (110)/(200) and (203) diffractions (Figure 4a), the maximum intensity of (110)/(200) diffraction was found to locate at 3 and 183°, whereas that of (203) diffraction was at 32, 152, 213, and 332°, indicating that the angle between these two planes was 30.2°, which was consistent with that calculated from the reported unit cell of α-form PLLA crystal.[46] Furthermore, we could identify a weak (002) diffraction situating orthogonally to (110)/(200) diffraction in the lower q region, as marked in Figure 4b. Because the a axis of the PLLA unit cell was parallel (according to the tangential- and radial-view patterns) or randomly distributed (manifested from the top-view pattern) with respect to the lamellar interface and the crystallographic c-axis was found to be parallel to the lamellar normal, the PLLA crystalline stems were deduced to orient parallel to the lamellar normal (or perpendicular to the lamellar interface). Such a homeotropic orientation of PLLA crystals was in accord with the previous results of crystalline−amorphous PLLA-containing diblock copolymer systems.[15]

The diffraction arcs located at the third quadrant (q = 15.2 nm^{-1}) and the forth equator (q = 16.8 nm^{-1}) in Figure 3a,b are attributed to the (110) and (200) diffractions of PE crystals, respectively. The angle between these two planes was 56.3°, which was consistent with the orthorhombic unit cell of PE crystal.[47] Because the (200) diffraction of PE crystal was

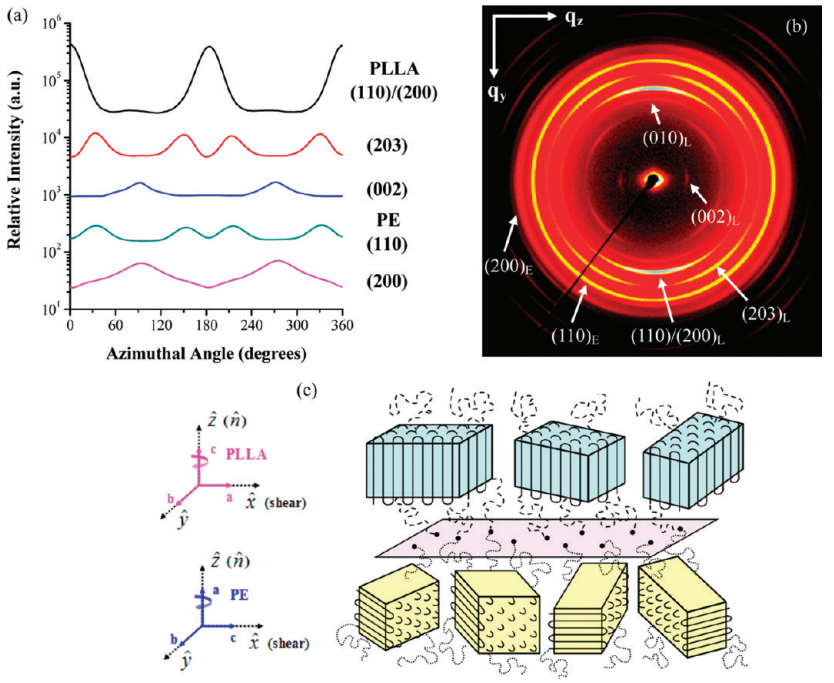

Figure 4. (a) Azimuthal scans of (110)/(200), (203), (002) diffractions of PLLA crystal and (110), (200) diffractions of PE crystal. (b) Identification of (002) diffraction of PLLA crystal in the lower q region of the 2D WAXD pattern. (The subscripts L and E marked in the (*hkl*) diffraction planes signify PLLA and PE, respectively.) (c) Schematic presentation of orthogonal crystal orientation with homeotropic orientation of PLLA crystals and the homogeneous orientation of PE crystals in the lamellar microdomain.

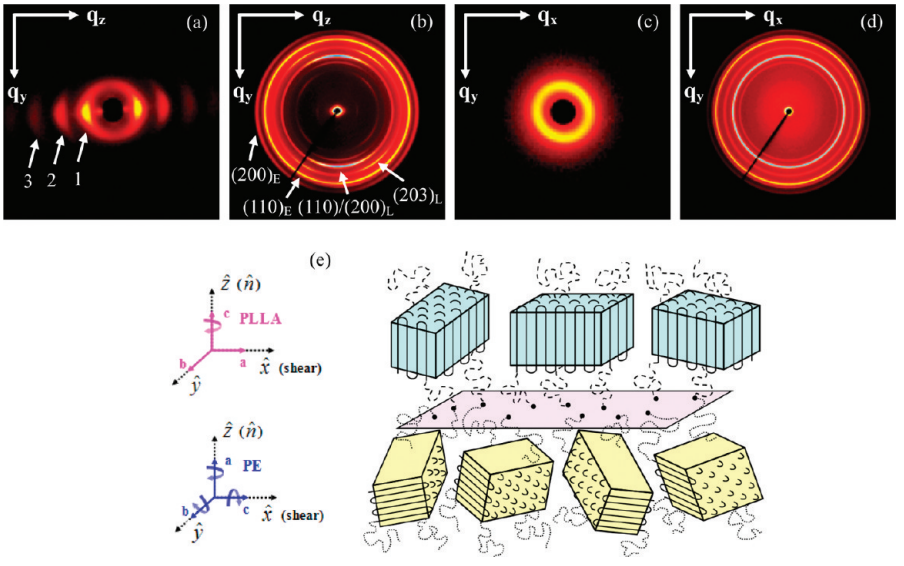

Figure 5. Two-dimensional SAXS/WAXD patterns of shear-oriented PLLA-*b*-PE subjected to a two-stage crystallization process with a large undercooling for the second stage. The system was cooled from 190 to 120 °C to allow PLLA crystallization, followed by cooling to T_c^{PE} = 40 °C to induce PE crystallization. (Similar scattering characteristics were observed for T_c^{PE} = −50−30 °C or direct immersion into liquid nitrogen.) (a) Tangential-view SAXS pattern; (b) tangential-view WAXD pattern (detailed azimuthal scans are shown in Figure S1(a) in the Supporting Information); (c) top-view SAXS pattern; (d) top-view WAXD pattern; and (e) schematic illustration of homeotropic orientation of PLLA crystals and the random orientation of PE crystals in the lamellar microdomain. The subscripts L and E marked in the (*hkl*) diffraction planes signify PLLA and PE, respectively.

found to locate at the equator in the tangential- and radial-view patterns, the crystalline stems of PE were deduced to align parallel to the lamellar interface; that is, the crystals showed the homogeneous orientation. This type of orientation has been prevalently observed among PE-based crystalline−amorphous diblock copolymers.[10−14,48] It appears that such a preference of PE crystal orientation was not perturbed by the crystalline nature of the connecting PLLA blocks (compared with the amorphous nature of the connecting blocks in the previous works). Consequently, the two-stage crystallization in PLLA-*b*-PE at

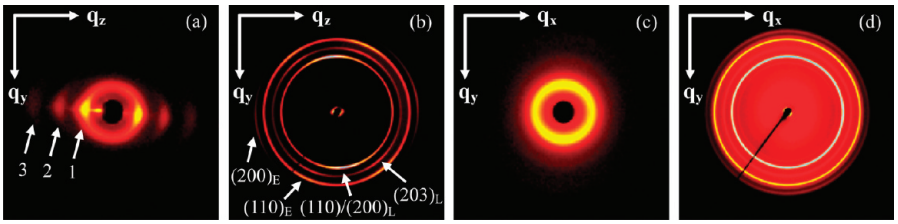

Figure 6. Two-dimensional SAXS/WAXD patterns of shear-oriented PLLA-*b*-PE subjected to a one-stage crystallization process with low undercooling. The system was directly quenched from T_c = 190 °C to T_c = 97 °C to induce competitive crystallization of PLLA and PE blocks. (Similar scattering patterns were observed for T_c = 80 °C.) (a) Tangential-view SAXS pattern; (b) tangential-view WAXD pattern (detailed azimuthal scans are shown in Figure S1(b) in the Supporting Information); (c) top-view SAXS pattern; and (d) top-view WAXD pattern. The subscripts L and E marked in the (*hkl*) diffraction planes signify PLLA and PE, respectively.

$T_c^{PE} \geq 45$ °C was able to generate an "orthogonal crystal orientation" with the crystalline stems of PLLA and PE oriented perpendicularly to each other, as schematically illustrated in Figure 4c.

Figure 5 shows the 2D SAXS/WAXD patterns of shear-oriented PLLA-*b*-PE subjected to a two-stage crystallization process where the crystallization of PE took place at a large undercooling (T_c^{PE} = 40 °C). Similar scattering characteristics were observed for lower T_c^{PE} values ($T_c^{PE} \cong -50$ to 30 °C) or for the sample directly quenched into liquid nitrogen from the melt. Because the 2D SAXS/WAXD patterns of tangential- and radial-view patterns were identical, only the tangential-view patterns were presented in Figure 5. The PLLA crystals formed at T_c^{PLLA} = 120 °C (i.e., during the first stage of the crystallization process) have already been shown to adopt homeotropic orientation. After quenching to a much lower crystallization temperature to induce PE crystallization, all PE diffractions became isotropic, as revealed in the 2D WAXD patterns (Figure 5b), indicating a random crystal orientation within the confined lamellae (Figure 5e). This random orientation is believed to arise from the extremely high nucleation density at large undercoolings. When a given nucleus appears within the lamellar microdomain, it should not feel the confinement effect because its dimension is much smaller than the lamellar thickness; consequently, most nuclei developed in the microdomain are randomly oriented.[9] At very large undercooling, where the nucleation is extremely rapid, a great number of nuclei explode in the microdomain abruptly; therefore, the microdomains are quickly filled with randomly oriented nuclei, and the crystal growth becomes highly frustrated by the jamming of these crystallites, leading eventually to crystals in random orientation.

Crystal Orientation Displayed under One-Stage Crystallization. Figure 6 shows a set of 2D SAXS/WAXD patterns of shear-oriented PLLA-*b*-PE subjected to a one-stage crystallization process at T_c = 97 °C. (Similar scattering patterns were observed for T_c = 80 °C.) The sample was directly cooled from 190 °C to the prescribed crystallization temperature to induce simultaneous and competing crystallization of PLLA and PE blocks. The 2D SAXS pattern was qualitatively identical to those obtained for the two-stage crystallization, but the interlamellar distance observed upon one-stage crystallization was slightly smaller. This minor discrepancy was attributed to the competition between crystallization rate of the leading block and the driving force of the microphase separation.[44] However, it was clear that both crystallization conditions eventually introduced an inappreciable perturbation of the melt morphology because the lamellar microdomains were still highly ordered and oriented parallel to the shear direction.

Our previous time-resolved SAXS/WAXS results have shown that the crystallization of PE block was faster than that of the PLLA block upon quenching to T_c in the one-stage crystallization process despite a larger undercooling for PLLA because PE is a very flexible polymer and can easily crystallize.[44] As a result, the one-stage crystallization performed here will yield PE as the leading crystallizing block that constructed a hard-confinement environment for PLLA blocks to crystallize. This fact provides an inverse scenario as compared with the two-stage crystallization. Even so, the scattering patterns observed for 80 ≤ T_c ≤ 97 °C were virtually identical to those displayed in Figure 3 (i.e., two-stage crystallization with lower undercoolings), showing that PLLA crystals still exhibited homeotropic orientation and PE crystals adopted homogeneous orientation, as illustrated in Figure 4c.

However, when the sample was crystallized at 70 °C (i.e., at a temperature only slightly higher than $T_g^{PLLA} \approx 62$ °C) from the melt, the isotropic WAXD pattern indicated that PLLA crystals became randomly oriented (Figure 7b). This again may be attributed to the high nucleation driving force that led to a burst in randomly oriented PLLA nuclei in the lamellar microdomains, as represented in Figure 7e.

Figures 8 and 9 show the 2D SAXS/WAXD patterns of shear-oriented PLLA-*b*-PE subjected to a one-stage crystallization process at T_c = 60 and 40 °C (where essentially identical scattering patterns were observed for lower T_c values), respectively. (Essentially identical scattering patterns were observed for lower T_c values.) As can be seen, when the system was crystallized with an even larger undercooling (i.e., $T_c \leq 60$ °C), the diffraction peaks of PLLA disappeared in all WAXD patterns. This result reflected that our quenching procedure was efficient, such that PLLA block could not crystallize immediately upon quenching from 190 °C to low crystallization temperatures ($T_c < T_g^{PLLA}$) and finally vitrified in the glassy state. For 45 ≤ T_c ≤ 60 °C (Figure 8b,d), PE crystals tend to show homogeneous orientation sandwiched between the glassy PLLA layers; however, the ring-like WAXD patterns of PE crystals were observed over a broad range of −50 ≤ T_c ≤ 40 °C or for the sample directly quenched in liquid nitrogen from the melt (as shown in Figure 9b,d), indicating that nearly random orientation of the PE crystals was produced between the glassy PLLA layers. It is worth noting that PE crystals still exhibited homogeneous orientation at T_c ranging from 60 to 45 °C ($< T_g^{PLLA}$) and started to show random orientation at $T_c \leq 40$ °C; this result strongly indicated that the onset of random orientation in PE microdomain was not related to the T_g of the covalently bonded PLLA block. As a result, such random orientation should stem from the extremely high nucleation density but not the transition from soft to hard

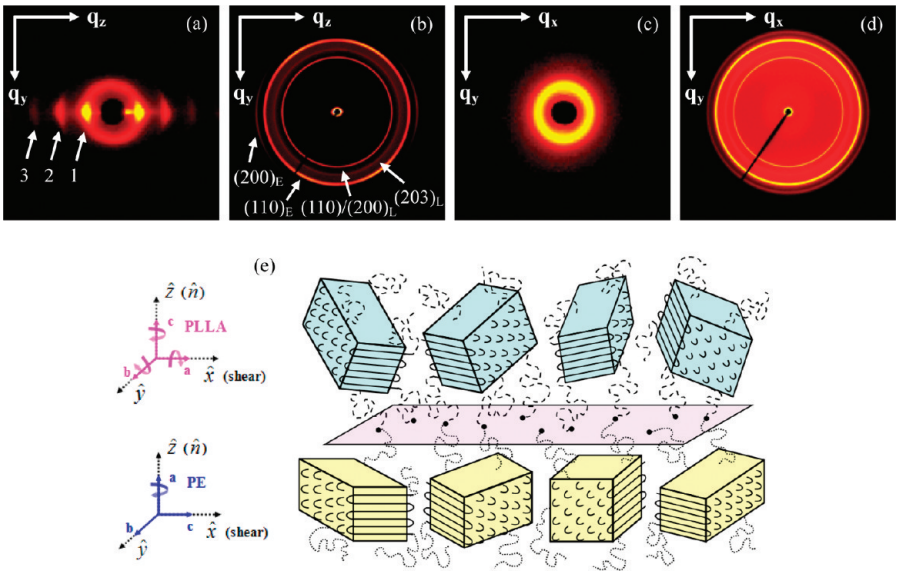

Figure 7. Two-dimensional SAXS/WAXD patterns of shear-oriented PLLA-*b*-PE subjected to a one-stage crystallization process. The system was directly quenched from 190 °C to T_c = 70 °C to induce competitive crystallization of PLLA and PE blocks. (a) Tangential-view SAXS pattern; (b) tangential-view WAXD pattern (detailed azimuthal scans are shown in Figure S1(c) in the Supporting Information); (c) top-view SAXS pattern; (d) top-view WAXD pattern; and (e) schematic illustration of random orientation of PLLA crystals and the homogeneous orientation of PE crystals in the lamellar microdomain. The subscripts L and E marked in the (*hkl*) diffraction planes signify PLLA and PE, respectively.

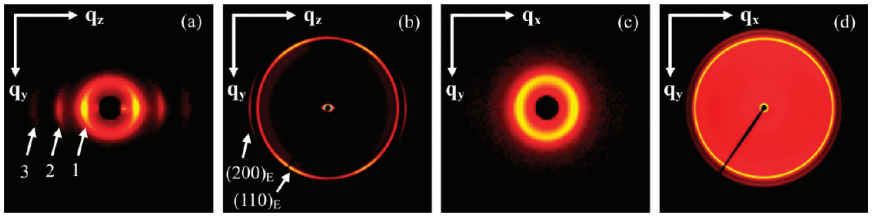

Figure 8. Two-dimensional SAXS/WAXD patterns of shear-oriented PLLA-*b*-PE subjected to a one-stage crystallization process. The system was directly quenched from T_c = 190 °C to 60 °C to induce PE crystallization. (Similar scattering characteristics were observed for T_c = 45 °C.) (a) Tangential-view SAXS pattern; (b) tangential-view WAXD pattern (detailed azimuthal scans are shown in Figure S1(d) in the Supporting Information); (c) top-view SAXS pattern; and (d) top-view WAXD pattern. The subscript E marked in the (*hkl*) diffraction planes signifies PE.

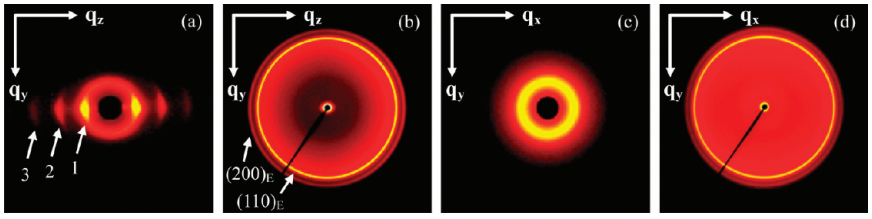

Figure 9. Two-dimenional SAXS/WAXD patterns of shear-oriented PLLA-*b*-PE subjected to a one-stage crystallization process with large undercooling. The system was directly quenched from T_c = 190 °C to 40 °C to induce PE crystallization. (Similar scattering characteristics were observed for T_c = −50−30 °C or direct immersion into liquid nitrogen.) (a) Tangential-view SAXS pattern; (b) tangential-view WAXD pattern (detailed azimuthal scans are shown in Figure S1(e) in the Supporting Information; (c) top-view SAXS pattern; and (d) top-view WAXD pattern. The subscript E marked in the (*hkl*) diffraction planes signifies PE.

confinement exerted by the neighboring PLLA blocks. It is interesting to note that homogeneous orientation of PE crystals was observed at $T_c > T_g^{PLLA}$ (i.e., 70 ≤ T_c ≤ 97 °C, where the temporarily amorphous PLLA imposed a soft confinement to PE crystallization) or $T_c < T_g^{PLLA}$ (i.e., 45 ≤ T_c ≤ 60 °C, where PLLA imposed a hard confinement to PE crystallization) in the one-stage crystallization. This was in accord with the previous study of PLLA-*b*-PS by Ho et al., showing that the PLLA crystal orientation was not influenced by the type of confinement exerted by the amorphous PS block.[15]

The dependence of crystal orientation on crystallization condition can be presented more quantitatively by Herman's orientation function (*f*), evaluated using the intensity distributions of (110)/(200) and (200) diffractions of PLLA and PE

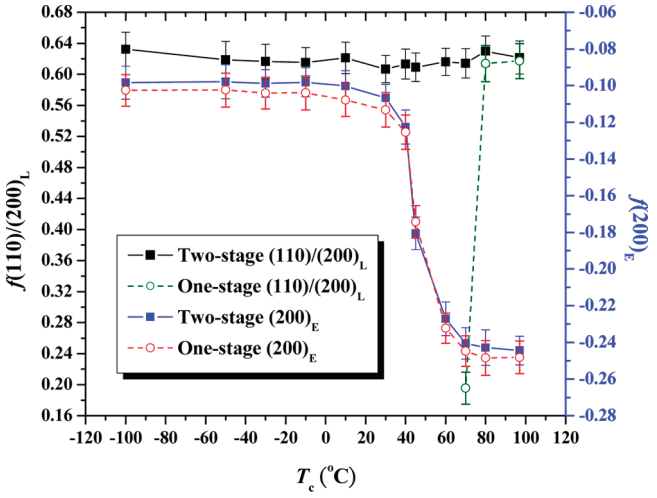

Figure 10. Herman's orientation function (f) calculated using the azimuthal distributions of the intensities of (110)/(200) and (200) diffractions for PLLA and PE crystals, respectively, as a function of crystallization temperature used for PE crystallization in two-stage crystallization (where PLLA crystallization was always induced at 120 °C) and for both PLLA and PE crystallizations in one-stage crystallization.

crystals, respectively, along the azimuthal angle (ϕ) of the 2-D scattering pattern.[49] For calculation of f, the tangential-view patterns were analyzed, and the $\hat{y}$ axis was taken as the reference direction; f has a value of 1.0 when the normal of the diffraction plane is parallel to the reference direction (i.e., $\phi = 0°$), a value of −0.5 means a perpendicular orientation of the diffraction plane normal to the reference direction (i.e., $\phi = 90°$), and a value of 0 signals random crystal orientation. f was calculated at each quadrant, followed by averaging four values to obtain f at each T_c. The dependences of the values of f for both PLLA and PE crystals under crystallization conditions are displayed in Figure 10. For two-stage crystallization, the value of f remained almost constant at ca. 0.63 for PLLA. In this case, the sample was always annealed at 120 °C to allow PLLA crystallization to saturation before cooling to the prescribed T_c to induce PE crystallization; therefore, the orientation of PLLA crystals thus formed was stable, essentially unaffected by the subsequent crystallization of PE block. With decreasing T_c the value of f of PE changed slightly with decreasing T_c at $45 < T_c \leq 60$ °C, but it increased abruptly across 40−45 °C. This revealed that with decreasing T_c PE crystal orientation changed abruptly from homogeneous to random at $T_c = 40-45$ °C. For one-stage crystallization, the value of f for PLLA remained approximately constant at $80 \leq T_c \leq 97$ °C, but it decreased sharply across 70−80 °C with decreasing T_c, indicating that the crystal orientation transformed abruptly from homeotropic to random. When T_c was <60 °C (where $T_c < T_g^{PLLA}$), the diffractions of PLLA crystals were not observable in all WAXD patterns because PLLA block was vitrified in the glassy state. The transformation of PE crystal orientation with respect to T_c in one-stage crystallization was quite similar to that found in two-stage crystallization, where the crystals did not show preferred orientation when T_c was <40 °C. Moreover, the dependence of PE crystal orientation on crystallization temperature found for the present double-crystalline PLLA-*b*-PE was almost in parallel to that observed for the crystalline−amorphous PE-*b*-PDLLA (where PDLLA is a racemic uncrystallizable block), which also exhibited a homogeneous-random transformation in crystal orientation at 40−45 °C.[48] We therefore concluded that the orientation behavior of PE crystals in PE-*b*-PLA diblock was governed mainly by the crystallization temperature but independent of the characteristics of the neighboring PLA block.

Because the rapid cooling from melt to $T_c \leq 40$ °C only induced PE crystallization to generate randomly oriented PE crystals, it is of interest to examine the orientation of the PLLA crystals formed by cold crystallization through heating these samples from the glassy state to $T_{re}^{PLLA} > T_g^{PLLA}$. Figure 11 and Figure S2 in the Supporting Information show the 2D SAXS/WAXD patterns of PLLA-*b*-PE directly quenched into liquid nitrogen from the melt, followed by heating to $T_{re}^{PLLA} = 70$ and 90 °C, respectively, to induce cold crystallization of PLLA blocks. In the case of $T_{re}^{PLLA} = 70$ °C, the orientation of PLLA crystals was found to be isotropic (cf. Figure 11b,d). This result demonstrated that the crystal orientation of PLLA was preserved irrespective of whether the crystallization occurred by cooling from the melt (cf. Figure 7b) or by heating from the glassy state (Figure 11b). The random crystal orientation of both PLLA and PE crystalline stems is schematically illustrated in Figure 11e. Once the cold crystallization temperature was increased to 90 °C, the homeotropic orientation of PLLA crystals was recovered, as evidenced by the preferred orientation of (110)/(200) and (203) diffractions (Figure S2 in the Supporting Information). The corresponding relative crystal orientations of PLLA and PE reverted back to the orthogonal type, as represented in Figure 5e.

Table 1 summarizes the dependence of crystal orientation on the thermal history and crystallization temperature with respect to the lamellar normal. Comparing our results with the literature results for the corresponding PLLA- or PE-containing crystalline−amorphous (C−A) diblocks (e.g., PLLA-*b*-PS, PE-*b*-PS, PE-*b*-PVCH, PE-*b*-PEE, PE-*b*-PEP, PE-*b*-PDLLA, etc.),[10−15,48] we found that the preferred crystal orientations of both PLLA and PE blocks in the present double-crystalline PLLA-*b*-PE system were identical to those of the two blocks in their respective C−A systems. In other words, PLLA crystals normally displayed homeotropic orientation, whereas homogeneous orientation mostly took place for PE crystals under the 1-D confinement established by the microphase separation in the melt. This observation led us to conclude that it was the strong segregation between the two blocks that allowed independent crystallization of each component regardless of whether the other covalently linked block can crystallize or not.

It is of interest to discuss why PLLA and PE crystals would exhibit orthogonal crystal orientation. Previous simulation work reported by Hu et al.[23] revealed that in the melt state the chain segments near the block interface possess orientational order due to the junction point constraint, leading to local segmental alignment parallel to the lamellar normal. Such a preferred segmental orientation would lead to homeotropic crystal orientation once the nucleation starts near the interfacial region. This simulation result thus predicts that homeotropic orientation is more thermodynamically favorable than homogeneous orientation. The homogeneous orientation predominantly observed in PE-based diblocks is apparently contradictory to this prediction; therefore, the persistence of homogeneous crystal orientation in PE-based block copolymers may be kinetic in origin.

Here we evoke a kinetic reasoning that postulates that the crystal orientation is governed by the competition between nucleation rate and crystal growth kinetics.[48] When the crystallization took place at a very low undercooling, the nucleation rate should be considerably slow. Hence, the crystal grown from a given

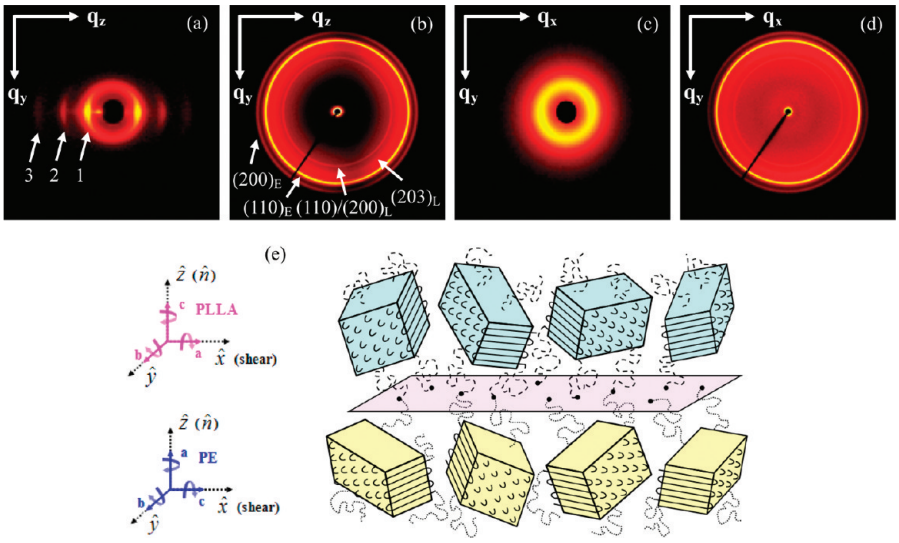

Figure 11. Two-dimensional SAXS/WAXD patterns of shear-oriented PLLA-*b*-PE subjected to a one-stage crystallization process, followed by reheating to a temperature higher than T_g^{PLLA}. The system was directly quenched from 190 °C into liquid nitrogen to allow for PE crystallization, followed by reheating to T_{re}^{PLLA} = 70 °C to induce crystallization of PLLA blocks from the glassy state. (a) Tangential-view SAXS pattern; (b) tangential-view WAXD pattern (detailed azimuthal scans are shown in Figure S1(f) in the Supporting Information); (c) top-view SAXS pattern; (d) top-view WAXD pattern; and (e) schematic illustration of random orientation of both PLLA and PE crystals in the lamellar microdomain. The subscripts L and E marked in the (*hkl*) diffraction planes signify PLLA and PE, respectively.

Table 1. Dependence of Crystal Orientation on Thermal History and Crystallization Temperature with Respect to the Lamellar Normal[a]

	PLLA-*b*-PE			
	two-stage crystallization		one-stage crystallization	
sample temperature	PLLA	PE	PLLA	PE
97 °C	⊥	∥	⊥	∥
80 °C	⊥	∥	⊥	∥
70 °C	⊥	∥	O	∥
60 °C	⊥	∥		∥
45 °C	⊥	∥		∥
40 °C	⊥	O		O
30 °C	⊥	O		O
10 °C	⊥	O		O
−10 °C	⊥	O		O
−30 °C	⊥	O		O
−50 °C	⊥	O		O
liquid N_2	⊥	O		O
liquid N_2 reheat to 70 °C			O	O
liquid N_2 reheat to 90 °C			⊥	O

[a] ⊥ denotes the homeotropic crystal orientation, where the *c*-axis orientation is parallel to $\hat{n}$; ∥ signals the homogeneous crystal orientation, where the *c*-axis orientation is perpendicular to lamellar normal $\hat{n}$; and O indicates isotropic orientation, where the *c*-axis orientation is randomly distributed with respect to $\hat{n}$.

nucleus may not feel the interference from another crystal before the growth front impinges the interface of the lamellar microdomain. In this case, the crystal would adjust its orientation to facilitate long-range growth and eventually adopt homeotropic orientation.

At a larger undercooling, where the nucleation density becomes quite high (but is not exceedingly high to abruptly fill the microdomain with randomly oriented nuclei), the growing crystals, which are disk or lamellae in shape, may experience an excluded volume interaction when two of them are sufficiently close. This is reminiscent of the interaction between discotic liquid crystalline molecules that gives rise to a regular stacking of the molecules to form a columnar mesophase. Once this type of interaction is significant, the crystals should stack along the lamellar interface to generate a homogeneous crystal orientation.

On the basis of our kinetic reasoning, the preferred homogeneous orientation of PE-containing diblocks may thus be attributed to the higher nucleation power of PE block (comparing with that of PLLA) in the lamellar microdomain. It has been found that homogeneous nucleation of PE was able to take place at a relatively small critical degree of undercooling ($\Delta T_{cr} \approx 40$ K)[50,51] in comparison with other semicrystalline polymers (e.g., $T_{cr} \approx 90$ K for PEO; $T_{cr} \approx 100$ K for PCL) in block copolymer systems.[52,53] It is also well known that even in the bulk polyethylene has an intrinsically high density of active nuclei (on the order of 10^9 nuclei/cm^3, at least three orders of magnitude larger than PEO and PCL).[50,54] All of the above suggests that PE indeed has an excellent nucleating power and may lead to the persistence of homogeneous orientation in the diblock copolymers.

Finally, we would like to note that the T_c range (i.e., 40−45 °C) at which the transition from homogeneous to random orientation of PE crystals in the present PLLA-*b*-PE occurred in one-stage crystallization was in the vicinity of the T_g of PLLA, which implied that vitrification of the amorphous block may play a role in causing random crystal orientation. Because the crystal growth should involve a relatively long-range transport of PE segments to the growth front, the growth of PE crystals may become highly frustrated because of the great constraint of the diffusion of junction points at the interface while PE is anchored

to the glassy PLLA microdomain. In this case, nucleation could dominate the crystallization more easily and consequently lead to random orientation of the crystals.

CONCLUSIONS

Orientation of crystals formed within the lamellar microdomains of a double-crystalline PLLA-*b*-PE has been investigated by means of 2D SAXS/WAXD techniques. Utilizing two- and one-stage crystallization histories, the variations of crystal orientation under sequential and competitive crystallization have been systematically investigated. The orientation of PLLA crystals always displayed homeotropic orientation with the crystalline stems lying parallel to the lamellar normal; on the other hand, a homogeneous crystal orientation with the crystalline stems oriented parallel to the interface was widely observed under low-to-moderate undercoolings for PE. As a result, PLLA and PE crystals predominantly exhibited an orthogonal orientation, except at very large undercooling or at T_c values near T_g^{PLLA}. The fact that the preferred crystal orientations were not affected by the crystallization history and were identical to those observed for corresponding C−A diblock systems indicated that PLLA and PE blocks crystallized independently in their respective microdomains as a consequence of the strong segregation strength between them.

ASSOCIATED CONTENT

Supporting Information. The azimuthal scans of (110)/(200), (203) diffractions of PLLA crystal and (110), (200) diffractions of PE crystal under various crystallization conditions. Two- dimensional SAXS/WAXD patterns of shear-oriented PLLA-*b*-PE subjected to a one-stage crystallization process followed by reheating to a temperature higher than T_g^{PLLA}. The system was directly quenched from 190 °C into liquid nitrogen to allow for PE crystallization followed by reheating to T_{re}^{PLLA} = 90 °C to induce crystallization of PLLA blocks from the glassy state. This material is available free of charge via the Internet at http://pubs.acs.org.

AUTHOR INFORMATION

Corresponding Author

*E-mail: hlchen@che.nthu.edu.tw (H.-L.C.); amuller@usb.ve (A.J.M.).

ACKNOWLEDGMENT

We acknowledge Marc A. Hillmyer for providing the block copolymers used in this study. We thank Kelly Anderson for the synthesis of the block copolymers and Marc Rodwogin for his help with an initial morphology determination by SAXS. We also thank to the National Synchrotron Radiation Center at BL23A1 and BL17A1 for supporting us in carrying out all of the experiments. Finally, we acknowledge the support from the National Science Council under grant NSC 99-2221-E-007-008 and from the Frontier Center of Fundamental and Applied Sciences of Matters of the National Tsing Hua University.

REFERENCES

(1) Park, M.; Harrison, C.; Chaikin, P. M.; Register, R. A.; Adamson, D. H. *Science* **1997**, *276*, 1401–1404.
(2) Huang, E.; Rockford, L.; Russell, T. P.; Hawker, C. J. *Nature (London)* **1998**, *395*, 757–758.
(3) Zalusky, A. S.; Olayo-Valles, R.; Taylor, C. J.; Hillmyer, M. A. *J. Am. Chem. Soc.* **2001**, *123*, 1519–1520.
(4) Bates, F. S.; Fredrickson, G. H. *Annu. Rev. Phys. Chem.* **1990**, *41*, 525–557.
(5) Hamley, I. W. *The Physics of Block Copolymers*; Oxford University Press: New York, 1998; Chapter 5.
(6) De Rosa, C.; Park, C.; Thomas, E. L.; Lotz, B. *Nature (London)* **2000**, *405*, 433–437.
(7) Whitesides, G. M.; Grzybowski, B. *Science* **2002**, *295*, 2418–2421.
(8) Müller, A. J.; Balsamo, V.; Arnal, M. L. *Adv. Polym. Sci.* **2005**, *190*, 1–63.
(9) Zhu, L.; Cheng, S. Z. D.; Calhoun, B. H.; Ge, Q.; Quirk, R. P.; Thomas, E. L.; Hsiao, B. S.; Yeh, F. J.; Lotz, B. *J. Am. Chem. Soc.* **2000**, *122*, 5957–5967.
(10) Douzinas, K. C.; Cohen, R. E. *Macromolecules* **1992**, *25*, 5030–5035.
(11) Cohen, R. E.; Bellare, A.; Drzewinski, M. A. *Macromolecules* **1994**, *27*, 2321–2323.
(12) Kofinas, P.; Cohen, R. E. *Macromolecules* **1994**, *27*, 3002–3008.
(13) Hamely, I. W.; Fairclough, J. P. A.; Terrill, N. J.; Ryan, A. J.; Lipic, P. M.; Bates, F. S.; Towns-Andrews, E. *Macromolecules* **1996**, *29*, 8835–8843.
(14) Myers, S. B.; Register, R. A. *Macromolecules* **2010**, *43*, 393–401.
(15) Ho, R. M.; Lin, F. H.; Tsai, C. C.; Lin, C. C.; Ko, B. T.; Hsiao, B. S.; Sics, I. *Macromolecules* **2004**, *37*, 5985–5994.
(16) Sun, Y. S.; Chung, T. M.; Li, Y. J.; Ho, R. M.; Ko, B. T.; Jeng, U. S.; Lotz, B. *Macromolecules* **2006**, *39*, 5782–5788.
(17) Quiram, D. J.; Register, R. A.; Marchand, G. R. *Macromolecules* **1997**, *30*, 4551–4558.
(18) Loo, Y. L.; Register, R. A.; Adamson, D. H. *Macromolecules* **2000**, *33*, 8361–8366.
(19) Huang, P.; Zhu, L.; Cheng, S. Z. D.; Ge, Q.; Quirk, R. P.; Thomas, E. L.; Lotz, B.; Hsiao, B. S.; Liu, L. Z.; Yeh, F. J. *Macromolecules* **2001**, *34*, 6649–6657.
(20) Nojima, S.; Ohguma., Y.; Kadena, K.; Ishizone, T.; Iwasaki, Y.; Yamaguchi, K. *Macromolecules* **2010**, *43*, 3916–3923.
(21) Hsiao, M. S.; Zheng, J. X.; Leng, S.; Van Horn, R. M.; Quirk, R. P.; Thomas, E. L.; Chen, H. L.; Hsiao, B. S.; Rong, L.; Lotz, B.; Cheng, S. Z. D. *Macromolecules* **2008**, *41*, 8114–8123.
(22) Hsiao, M. S.; Zheng, J. X.; Van Horn, R. M.; Quirk, R. P.; Thomas, E. L.; Chen, H. L.; Lotz, B.; Cheng, S. Z. D. *Macromolecules* **2009**, *42*, 8343–8352.
(23) Hu, W. B.; Frenkel, D. *Faraday Discuss.* **2005**, *128*, 253–260.
(24) Müller, A. J.; Balsamo, V.; Arnal, M. L. In *Lecture Notes in Physics: Progress in Understanding of Polymer Crystallization*; Reiter, G., Strobl, G., Eds.; Springer Lecture Notes in Physics 714; Springer: Berlin, 2007; pp 229−259.
(25) Castillo, R. V.; Müller, A. *J. Prog. Polym. Sci.* **2009**, *34*, 516–560.
(26) Kim, K. S.; Chung, S.; Chin, I. J.; Kim, M. N.; Yoon, J. S. *J. Appl. Polym. Sci.* **1999**, *72*, 341–348.
(27) Maglio, G.; Migliozzi, A.; Palumbo, R. *Polymer* **2003**, *44*, 369–375.
(28) Sun, L.; Liu, Y. X.; Zhu, L.; Hsiao, B. S.; Avila-Orta, C. A. *Polymer* **2004**, *45*, 8181–8193.
(29) Nojima, S.; Akutsu, Y.; Washino, A.; Tanimoto, S. *Polymer* **2004**, *45*, 7317–7324.
(30) Hamley, I. W.; Castelletto, V.; Castillo, R. V.; Müller, A. J.; Martin, C. M.; Pollet, E.; Dubois, P. *Macromolecules* **2005**, *38*, 463–472.
(31) Castillo, R. V.; Arnal, M. L.; Müller, A. J.; Hamley, I. W.; Castelletto, V.; Schmalz, H.; Abetz, V. *Macromolecules* **2008**, *41*, 879–889.
(32) Cao, W. Y.; Tashiro, K.; Hanesaka, M.; Takeda, S.; Masunaga, H.; Sasaki, S.; Takata, M. *J. Phys. Chem. B* **2009**, *113*, 2338–2346.
(33) Kim, J. K.; Park, D. J.; Lee, M. S.; Ihn, K. J. *Polymer* **2001**, *42*, 7429–7441.
(34) Nojima, S.; Ono, M.; Ashida, T. *Polym. J.* **1992**, *24*, 1271–1280.

(35) Gan, Z. H.; Jiang, B. Z.; Zhang, J. *J. Appl. Polym. Sci.* **1996**, *59*, 961–967.
(36) Bogdanov, B.; Vidts, A.; Schacht, E.; Berghmans, H. *Macromolecules* **1999**, *32*, 726–731.
(37) Shiomi, T.; Imai, K.; Takenaka, K.; Takeshita, H.; Hayashi, H.; Tezuka, Y. *Polymer* **2001**, *42*, 3233–3239.
(38) Albuerne, J.; Marquez, L.; Müller, A. J.; Raquez, J. M.; Degee, P.; Dubois, P.; Castelletto, V.; Hamley, I. W. *Macromolecules* **2003**, *36*, 1633–1644.
(39) Takeshita, H.; Fukumoto, K.; Ohnishi, T.; Ohkubo, T.; Miya, M.; Takenaka, K.; Shiomi, T. *Polymer* **2006**, *47*, 8210–8218.
(40) Nojima, S.; Fukagawa, Y.; Ikeda, H. *Macromolecules* **2009**, *42*, 9515–9522.
(41) Wang, Y. B.; Hillmyer, M. A. *J. Polym. Sci., Part A: Polym. Chem.* **2001**, *39*, 2755–2766.
(42) Müller, A. J.; Castillo, R. V.; Hillmyer, M. *Macromol. Symp.* **2006**, *242*, 174–181.
(43) Müller, A. J.; Lorenzo, A. T.; Castillo, R. V.; Arnal, M. L.; Boschetti-De-Fierro, A.; Abetz, V. *Macromol. Symp.* **2006**, *245*, 154–160.
(44) Castillo, R. V.; Müller, A. J.; Lin, M. C.; Chen, H. L.; Jeng, U. S.; Hillmyer, M. A. *Macromolecules* **2008**, *41*, 6154–6164.
(45) Jeng, U. S.; Su, C. H.; Su, C. J.; Liao, K. F.; Chuang, W. T.; Lai, Y. H.; Chang, J. W.; Chen, Y. J.; Huang, Y. S.; Lee, M. T.; Yu, K. L.; Lin, J. M.; Liu, D. G.; Chang, C. F.; Liu, C. Y.; Chang, C. H.; Liang, K. S. *J. Appl. Crystallogr.* **2010**, *43*, 110–121.
(46) Hoogsteen, W.; Postema, A. R.; Pennings, A. J.; ten Brinke, G.; Zugenmaier, P. *Macromolecules* **1990**, *23*, 634–642.
(47) Zugenmaier, P.; Cantow Hans, J. *Kolloid Z. Z. Polym.* **1969**, *230*, 229–236.
(48) Lin, M. C.; Wang, Y. C.; Chen, H. L.; Müller, A. J.; Su, C. J.; Jeng, U. S. *J. Phys. Chem. B* **2011**, *115*, 2494–2502.
(49) Alexander, L. E. *X-ray Diffraction in Polymer Science*; Wiley: New York, 1969.
(50) Müller, A. J.; Balsamo, V.; Arnal, M. L.; Jakob, T.; Schmalz, H.; Abetz, V. *Macromolecules* **2002**, *35*, 3048–3058.
(51) Loo, Y. L.; Register, R. A.; Ryan, A. J. *Phys. Rev. Lett.* **2000**, *84*, 4120–4123.
(52) Chen, H. L.; Wu, J. C.; Lin, T. L.; Lin, J. S. *Macromolecules* **2001**, *34*, 6936–6944.
(53) Hsu, J. Y.; Hsieh, I. F.; Nandan, B.; Chiu, F. C.; Chen, J. H.; Jeng, U. S.; Chen, H. L. *Macromolecules* **2007**, *40*, 5014–5022.
(54) Arnal, M. L.; Matos, M. E.; Morales, R. A.; Santana, O. O.; Müller, A. J. *Macromol. Chem. Phys.* **1998**, *199*, 2275–2298.